A Stochastic Dynamics Simulation Study Associated with Hydration Force and Friction Memory Effect

Ben Zhuo Lu,[†,‡] Cun Xin Wang,*[,†] Wei Zu Chen,[†] Shun Zhou Wan,[‡,§] and Yun Yu Shi[‡]

Center for Biomedical Engineering, Beijing Polytechnic University, Beijing 100022, People's Republic of China, and School of Life Science, University of Science and Technology of China, Hefei 230026, People's Republic of China

Received: December 10, 1999; In Final Form: March 22, 2000

A new simulation approach for combining hydration force with generalized Langevin dynamics is developed in this paper. The exponential model is taken for the friction kernel. The hydration force determined by the boundary elementary method is taken into account as the mean force terms of the solvent, including the Coulombic interactions with the induced surface charge and the surface pressure of solvent. All simulations were performed on cyclic undecapeptide cyclosporin A (CPA). The simulation results obtained using the new method were analyzed and compared with those obtained using other methods, such as molecular dynamics simulations, generalized Langevin dynamics simulations, and conventional stochastic dynamics simulations. We found that the results obtained with the new method presented in this study show obvious improvements over the other simulation techniques and that the hydration force and friction relaxation together contribute to this improvement.

Introduction

Molecular dynamics (MD) simulations have been widely used to study the structural and dynamic properties of molecular systems.[1,2] However, there exist at least two limitations on this approach:[1] the approximation in the potential energy functions and the lengths of the simulations. The first limitation leads to systematic errors, and the second to statistical errors. Some previous studies have been performed to improve the form of potential functions.[3−5] To prolong the simulation time, the use of stochastic dynamics (SD) based on the Langevin equation is a recommended approach in which only the relevant portion of the molecule is considered explicitly and the remainder of the system, such as the solvent, serves to provide an effective potential, a friction drag, and a heat bath.[7] The friction memory effect is taken into account in generalized Langevin dynamics (GLD), which is a more proper approach when the solvent and solute particles have similar sizes and masses.

A potential of mean force of solvation that describes the average solvent effect on the solute degrees of freedom has important influence on the solute conformation.[5] However, conventional SD and GLD simulations have usually omitted the extra mean force terms of the solvent such as the Coulombic interaction with the induced surface charge and the boundary pressure exerted by the solvent.[7,8,10,12] Many efforts have been made to incorporate solvent effects into molecular mechanics or MD simulations using the Poisson−Boltzmann equation.[8−11] Recently, Wang and co-workers succeeded in incorporating the hydration force determined by the boundary elementary method (BEM)[13] into conventional SD simulations (SDBEM).[4] Then, Wan and co-workers used an exponential model for the friction kernel and developed the leapfrog algorithm for numerical integration of generalized Langevin dynamics.[12] Until now, however, no one has reported an efficient approach to incorporating both hydration force and friction memory into SD simulations for biomolecules. The present work is a continuation of the work developed by Wang et al.[4] The goal of this work is to develop a new simulation approach to GLD with a potential of mean force calculated by the BEM (GLDBEM) and to clarify how the hydration force and friction memory affect the conformational and dynamical behavior of the system in the GLDBEM simulation. Because we found that the original GLD algorithm by Wan et al.[12] may be subject to mathematical difficulty in actual calculations dealing with the stochastic terms in the simulation, the related parts of the GLD programs have been modified in the present study to solve such problems. To compare our simulation data with those obtained in the previous work, we have selected the same system, cyclosporin A (CPA), as our simulated system for examining the rationality and reliability of our GLDBEM approach.

Theory

For a system of N atoms, the GLD technique is based on the following generalized Langevin equation (GLE):

$$m_i\ddot{x}_i(t) = F_i(\{x_i(t)\}) - m_i \int_0^t \gamma_{i1}(t-\tau)\,\dot{x}_i(t)\,\mathrm{d}\tau + R_{i1}(t) \quad (1)$$

where x_i is the coordinate component and m_i the mass of the ith atom, $F_i(\{x_i(t)\})$ represents the system force, $\gamma_{i1}(t-\tau)$ is the friction kernel, and $R_{i1}(t)$ denotes the random force, which satisfies the fluctuation dissipation theorem[14]

* Author to whom correspondence should be addressed. E-mail: cxwang@bjpu.edu.cn.
† Beijing Polytechnic University.
‡ University of Science and Technology of China.
§ Present address: Laboratoire de Chimie Biophysique, Universite Louis Pasteur ISIS 4, rue Blaise Pascal, 67000 Strasbourg, France.

10.1021/jp994349o CCC: $19.00
Published on Web 06/28/2000

$$\langle R_{i1}(0)R_{i1}(t)\rangle = m_i k_B T \gamma_{i1}(t) \tag{2}$$

where the angular brackets indicate an ensemble average, k_B is the Boltzmann constant, and T is the absolute temperature.

The Laplace transform of the higher-order memory function $\gamma_{in}(t)$ can be expressed by the continued fraction equation[15]

$$\tilde{\gamma}_1(s) = \frac{\gamma_1(0)}{s + \tilde{\gamma}_2(s)} = \cfrac{\gamma_1(0)}{s + \cfrac{\gamma_2(0)}{s + \cfrac{\gamma_3(0)}{s + \ldots}}} \tag{3}$$

where $\gamma_n(t)$ is the nth order memory function and $\tilde{\gamma}_n(s)$ the Laplace transform of $\gamma_n(t)$. If the continued fraction in eq 3 is truncated at $n = 2$, the Laplace transform of $\gamma_1(t)$ can be written as

$$\tilde{\gamma}_1(s) = \frac{\gamma_1(0)}{s + 1/\tau_0} \tag{4}$$

Thus, the second-order of the memory function is $\gamma_2(t) = 1/\tau_0\ \delta(t)$, and the original function of the Laplace transform $\tilde{\gamma}_1(s)$ has an exponential form

$$\gamma_{i1}(t) = \gamma_{i0} \exp(-t/\tau_0) \tag{5}$$

where τ_0 is the relaxation time of the friction kernel and γ_{i0} is its initial value. Therefore, the exponential model for the friction kernel in eq 5 is also taken in this work as a simple approximate form. In this case, the leapfrog algorithm[16] can be used for numerical integration of the GLE with the exponential model for the friction kernel, and the numerical integration formula and procedure of GLD can be found in ref 12.

Here, we should point out that some modifications are made in our present work. The leapfrog algorithm was adopted in our work for the integration of eq 1. Therefore, there are two sets of random variables of $W_n(-\Delta t/2)$, $X_{n-1/2}(\Delta t/2)$, $V_n(-\Delta t/2)$ and $W_n(\Delta t/2)$, $X_{n+1/2}(-\Delta t/2)$, $V_n(\Delta t/2)$ in the leapfrog algorithm, in which W is a random variable with a Gaussian distribution and X and V are random variables appearing in the integration expressions for the position and velocity, respectively.[12] Each set of random variables obeys a trivariate Gaussian distribution[17]

$$f(s_1,s_2,s_3) = \frac{1}{(2\pi)^{3/2}|\mathbf{B}|^{1/2}} \times \exp\left\{-\frac{1}{2}(\mathbf{S}-\mathbf{M})^T \mathbf{B}^{-1} (\mathbf{S}-\mathbf{M})\right\} \tag{6}$$

where $\mathbf{S}$ is the random vector whose components are the random variables of s_1, s_2, and s_3 and $\mathbf{M}$ is the corresponding mean vector, $\mathbf{M} = \langle \mathbf{S} \rangle$. $\mathbf{B}$ is the covariance matrix $[\sigma_{ij}]$, $\sigma_{ij} = \langle s_i s_j \rangle^{1/2}$, and $|\mathbf{B}|$ its determinant. In practical calculations, we have found that the determinant $|\mathbf{B}|$ of the positive determined matrix B may be given by a negative value because of the calculating precision of the simulation. To solve this problem, we used power expansions for the matrix elements. For instance, the matrix element of $\mathbf{B}$ for the first set of random variables, σ_2^2, has the form (see eq B2 in Appendix B of ref 12)

$$\sigma_2^2 = \langle X_{n-1/2}^2(\Delta t/2)\rangle = \left[m\xi^2\left(1 - \frac{1}{\xi\tau_0}\right)\right]^{-2} \frac{m\gamma_0 k_B T}{\tau_0} \times \left\{(\xi\tau_0)^2\left[\Delta t/2 - 2\tau_0(1 - \exp(-\Delta t/2\tau_0)) + \frac{\tau_0}{2}(1 - \exp(-\Delta t/\tau_0))\right] - 2\xi\tau_0[\Delta t/2 - \tau_0(1 - \exp(-\Delta t/2\tau_0)) - \xi^{-1}(1 - \exp(-\xi\Delta t/2)) + (\xi + 1/\tau_0)^{-1} \times (1 - \exp(-\Delta t/2\tau_0)\exp(-\xi\Delta t/2))] + \Delta t/2 - 2\xi^{-1}[1 - \exp(-\xi\Delta t/2)] + (2\xi)^{-1}[1 - \exp(-\xi\Delta t)]\right\} \tag{7}$$

where

$$\xi \cong \gamma_0\tau_0[1 - \exp(-\Delta t/t_0)] \tag{8}$$

When we used the power expansions for the matrix elements, the power expansion form of σ_2^2 can be given by

$$\sigma_2^2 = \langle X_{n-1/2}^2(\Delta t/2)\rangle = \left[m\xi^2\left(1 - \frac{1}{\xi\tau_0}\right)\right]^{-2} \frac{m\gamma_0 k_B T}{\tau_0}\left[\frac{(\Delta t)^5}{640}\left(\xi^4 - 2\frac{\xi^3}{\tau_0} + \frac{\xi^2}{\tau_0^2}\right) - \frac{(\Delta t)^6}{2304}\left(\xi^5 - \frac{\xi^4}{\tau_0} - \frac{\xi^3}{\tau_0^2} + \frac{\xi^2}{\tau_0^3}\right) + \frac{(\Delta t)^7}{64512}\left(5\xi^6 - 3\frac{\xi^5}{\tau_0} - 4\frac{\xi^3}{\tau_0^2} - 3\frac{\xi^3}{\tau_0^2} + 5\frac{\xi^2}{\tau_0^4}\right)\right] + \ldots \tag{9}$$

A similar operation on the other elements of matrix $\mathbf{B}$ can be done in the same way. When we used this procedure in this work, the problem with calculating the value of the determinant $|\mathbf{B}|$ mentioned above was solved.

The system force $F_i(\{x_i(t)\})$ in eq 1 can be written as

$$F_i(t) = -\partial V_{mean}(\{x_i\})/\partial x_i \tag{10}$$

where V_{mean} is the system potential of mean force. In the present work, V_{mean} can be expressed as

$$V_{mean}(\{x_i\}) = V_{int}(\{x_i\}) + V_{sol}(\{x_i\}) \tag{11}$$

where V_{int} refers to the internal potential of solute atoms in the system and V_{sol} is the potential of mean force from the solvent. Hence, the system force can be obtained using

$$F_i = -\frac{\partial V_{int}(\{x_i\})}{\partial x_i} - \frac{\partial V_{sol}(\{x_i\})}{\partial x_i} = F_i^{int} + F_i^{sol} \tag{12}$$

where F_i^{int} is the force due to the simulated atoms of the system and F_i^{sol} is the hydration force due to the environment solvent. In this work, the hydration force F_i^{sol} is calculated using the classical continuum model of electrostatic interactions, which includes two parts: one is the Coulombic interaction with the induced surface charge, and the other is a purely mechanical boundary pressure of the solvent.[8,10] The hydration force is calculated by the BEM in this study. Because the detailed procedure of the BEM can be found in many other works,[13,18−20] here, we only give the main equations used in this study.

The interior potential ϕ^i and the exterior potential ϕ^e are the solutions of the Poisson equation and the linearized Poisson Boltzmann equation, respectively.

$$\nabla^2\phi_p^i = -\frac{1}{D_i}\sum_k q_k\,\delta(\mathbf{r_p}-\mathbf{r_k}) \tag{13}$$

$$\nabla^2\phi_p^e = k^2\phi^e(\mathbf{r_p}) \tag{14}$$

where D_i is the dielectric constant of the molecular interior, $\mathbf{r_p}$ is a point inside or outside the molecule, q_k is the kth point charge at $\mathbf{r_k}$, and k in eq 14 is the Debye inverse screening length. The solutions of eqs 13 and 14 can be written in the integral forms by using Green's second theorem on eqs 13 and 14.

$$\phi_p^i = \oint_S\left[G_{pk}\frac{\partial\phi_k^i}{\partial n} - \phi_k^i\frac{\partial G_{pk}}{\partial n}\right]dA_k + \frac{1}{D_i}\sum_k q_k G_{pk} \tag{15}$$

$$\phi_p^e = \oint_S\left[-u_{pk}\frac{\partial\phi_k^e}{\partial n} + \phi_k^e\frac{\partial u_{pk}}{\partial n}\right]dA_k \tag{16}$$

where the integration is taken over the entire molecular surface, k is a point on the surface, p is a point inside or outside the molecule, and $\mathbf{n}$ is the outward unit normal to the surface. The fundamental solution of eqs 13 and 14 can be expressed as

$$G_{pq} = \frac{1}{4\pi r_{pq}} \tag{17}$$

$$u_{pq} = \exp(-kr_{pq})/4\pi r_{pq} \tag{18}$$

where r_{pq} is the distance between points p and q. When the jump discontinuity of the double-layer potential at the boundary S is considered,[18] eqs 15 and 16 can be written as

$$\frac{1}{2}\phi_p^i = \oint_S\left[G_{pk}\frac{\partial\phi_k^i}{\partial n} - \phi_k^i\frac{\partial G_{pk}}{\partial n}\right]dA_k + \frac{1}{D_i}\sum_k q_k G_{pk} \tag{19}$$

$$\frac{1}{2}\phi_p^e = \oint_S\left[-u_{pk}\frac{\partial\phi_k^e}{\partial n} + \phi_k^e\frac{\partial u_{pk}}{\partial n}\right]dA_k \tag{20}$$

The surface potential and its normal derivatives can be evaluated from eqs 19 and 20 plus the following two boundary conditions:

$$\phi^i = \phi^e \tag{21}$$

$$D_i\frac{\partial\phi^i}{\partial n} = D_e\frac{\partial\phi^e}{\partial n} \tag{22}$$

where D_e is the dielectric constant of the solvent.

The electrostatic component of the hydration force acting on charge q_i is calculated with the expression

$$\mathbf{F}_i^{pol}(\mathbf{R}) = \oint_S\frac{q_i\sigma(\mathbf{r})(\mathbf{R}-\mathbf{r})}{|\mathbf{R}-\mathbf{r}|^3}\,d^2\mathbf{r} \tag{23}$$

where the integration is carried out over the entire molecular surface S and $\sigma(\mathbf{r})$ is the density of the induced polarization charge at an arbitrary point $\mathbf{r}$ on the molecular surface S. The relation between the $\sigma(\mathbf{r})$ and the exterior electric field $\mathbf{E}_e(\mathbf{r})$ is given by[19]

$$\sigma(\mathbf{r}) = \frac{1}{4\pi}\left(\frac{D_i - D_e}{D_i}\right)\mathbf{E}_e(\mathbf{r})\cdot\mathbf{n}(\mathbf{r}) \tag{24}$$

The purely mechanical boundary pressure acting on both the charged atom and the uncharged atoms on the surface can be calculated by the expression[8,10]

$$p(r_i) = \frac{1}{8\pi}(D_e - D_i)\left[(\mathbf{E}_e\cdot\mathbf{n})^2\left(\frac{D_e - D_i}{D_i}\right) + \left|\mathbf{E}_0\right|^2\right] \tag{25}$$

Thus, the force of solvent pressure on the ith atom is given by

$$\mathbf{F}_i^{press} = \int_S -\mathbf{n}p(\mathbf{r})\,d^2\mathbf{r} \tag{26}$$

where the integration is performed only over the portion of solvent accessible surface associated with the ith atom.

Computational Procedures

The hydration force and friction memory effect were incorporated into the conventional SD simulation technique simultaneously in this work by linking the BEM programs (MACBEM)[13] with the GLD program[12] based on the GROMOS package.[21] The program for calculating the hydration force on a charge and the solvent pressure based on the BEM were joined with the subroutine program FORCE in the GROMOS package. In the present work, the triangulation procedure in the BEM was similar to the method developed by Juffer and co-workers.[20] The molecular surface was defined as the center of the probe rolling around the molecule. The probe radius is 0.16 nm. The number of total triangles for CPA was 320.

In GLD, the atomic friction kernels satisfy the relation

$$\int_0^\infty \gamma(t)\,dt = \gamma_\tau\omega \tag{27}$$

where γ_τ is the friction constant, which was assigned a value of 91 ps^{-1} to represent the total solvent effect of water molecules,[7] and ω is an atomic accessible area weight factor, which is due to the degree of solute−solvent interaction. The calculation of ω usually uses the approximate expression

$$\omega = \max(0, 1 - N^{nb}/N^{nbref}) \tag{28}$$

where N^{nb} is the number of neigbour atoms of the concerned atom within a sphere of radius R^{nbref} and N^{nbref} is a reference number. In this work, we chose $N^{nbref} = 10$. The parameter R^{nbref} was set to 0.3 nm. The relaxation time, $\tau = 0.1$ ps, was used for the friction kernel,[12] and the initial friction coefficients, γ_{i0}, were taken to be 910 ps^{-2}, weighted with the accessible area factor.

The GROMOS force field[21] was used for all simulations. The initial structure of the CPA molecule used was the X-ray structure,[22] which is shown schematically in Figure 1. Nonpolar hydrogen atoms were included in the carbon atoms (united atom approach), while polar hydrogen atoms were treated explicitly. The system contained 90 atoms in total. The time step was taken to be 2 fs for integrating the equations of motion. A temperature bath and a pressure bath were applied to keep the system at 300 K and 1 atm.[24] All bond lengths were kept rigid using the SHAKE algorithm with a tolerance of 10^{-4}.[25]

The length of the simulation is one of the main concerns with protein dynamic simulations. Some recent studies suggested that a simulation length of 500 ps is acceptable. Daggett and Levitt pointed out that any solution simulation under 50 ps in duration is probably not sufficiently equilibrated for one to draw any conclusions about the behavior of proteins.[23] Because the previous MD, SD, and GLD simulations[4,6,7,12] were only performed for 40−60 ps, they seemed to be not long enough. In our work, after energy minimization, a 100-ps conventional

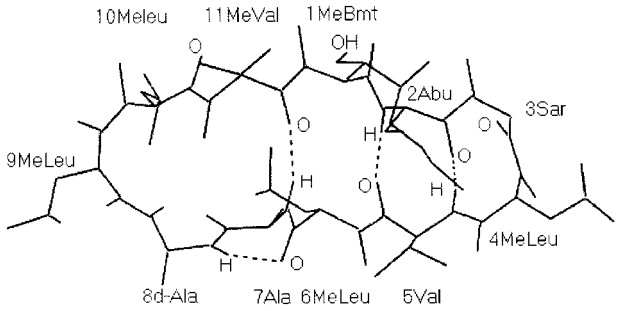

Figure 1. Schematic structure of cyclosporin A. The residue name of MeBmt is abbreviation for 4-(*E*-2-butenyl)-4,*n*-dimethylthreonine. The broken lines show the hydrogen-bonding network with high occupancies. A few of the atoms that contribute to the formation of the hydrogen bonds appearing in Table 2 are labeled, such that H refers to the hydrogen atom bonded to the nitrogen atom on the backbone and OH to the hydrogen atom in the hydroxyl group in 1MeBmt.

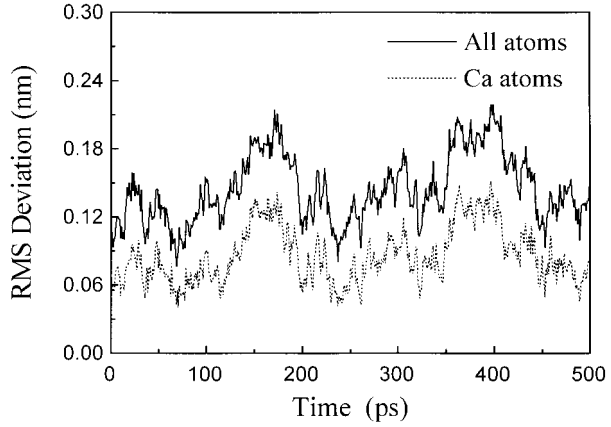

Figure 2. Root-mean-square deviation of atomic positions relative to the X-ray structure versus GLDBEM simulation time.

SD simulation was performed for system equilibration. Then, a 500-ps GLDBEM simulation was carried out, and the trajectories were saved every 25 time steps. For comparison, we also performed MD, GLD, and SD simulations again for 500 ps each. The trajectories from the last 400 ps of all simulations were used for analysis.

Results and Discussion

Position Fluctuation and Deviation. The root-mean-square (RMS) positional fluctuation and the RMS deviation of the generated structure from a reference structure as a function of time are important parameters for examining the molecular flexibility and the convergence of the simulations. Figure 2 shows the time-dependent RMS deviation of atomic positions in the GLDBEM simulation (after the 100-ps equilibration) relative to the X-ray crystal structure. As shown in Figure 2, the RMS shift in position has a stable value of 0.08−0.21 nm for all atoms and 0.04−0.14 nm for C_α atoms during the 500-ps simulation, which corresponds with the previous simulation work.[23] It is found that there are two small periodical peaks in Figure 2. The slight instability of the positional fluctuation can also be found in another study,[23] in which various patterns of positional fluctuation and deviation were reported and it was mentioned that the deviation could result from many different factors. Because the system can occur periodically with a slight reasonable deviation, the system seems to be in an equilibrium state after 100 ps of the GLDBEM simulation.

Table 1 lists the RMS atomic positional fluctuations and the mean anisotropy of atomic motion in CPA for the MD, SD, GLD, SDBEM, and GLDBEM simulations. The RMS positional fluctuation of our GLDBEM simulation is 0.078 nm for all atoms, which is larger than those of the SD (0.065 nm), GLD (0.074 nm), and SDBEM (0.075 nm) simulations and closer to that of the MD simulation (0.084 nm), which gives the largest positional fluctuation. This result is consistent with the recent simulation work by Fraternali and van Gunsteren.[5] Note that the value of the RMS fluctuations for the longer MD simulation (500-ps) is larger than that obtained from the previous short-time (50-ps) MD simulation (0.052 nm for all atoms and 0.036 nm for C_α atoms).[6] Daggett and Levitt have reported similar results obtained from different lengths of MD simulations for the different systems.[23] Generally, the RMS positional fluctuation in long simulations is larger. In the present work, the RMS positional fluctuation in the 500-ps MD simulation is the largest. This means that the CPA molecule shows more flexibility in the MD simulation in solution than in the other simulations without explicit solvent. As shown in Table 1, the values of the RMS fluctuations of the GLDBEM simulation are larger than those of the GLD simulation, and the RMS fluctuations of the SDBEM simulation are larger than those of the SD simulation. This means that the GLDBEM and SDBEM simulations can partially reflect the influence of the hydration force determined by the BEM. Comparing GLDBEM with SDBEM, and GLD with SD, it is found that the RMS fluctuations of the former simulations are larger than those of the latter simulations. This reflects the fact that the friction memory effect imposes an obvious influence on the motion of the molecular atoms. The mean anisotropy in the atomic motion in Table 1 is defined as the ratio of the shortest to the longest principal axis of the anisotropic fluctuation ellipsoids. The values for anisotropy are comparable for all five simulations.

TABLE 1: RMS Atomic Positional Fluctuations[a] and Mean Anisotropy for Atomic Motion in CPA

atom type	MD	SD	GLD	SDBEM	GLDBEM
			Positional Fluctuations		
all atoms	0.084	0.065	0.074	0.075	0.078
C_α atoms	0.052	0.040	0.044	0.044	0.049
MeLeu C_β	0.067	0.061	0.068	0.075	0.076
MeLeu C_γ	0.099	0.081	0.094	0.104	0.102
MeLeu C_δ	0.141	0.122	0.132	0.137	0.138
			Anisotropy		
all atoms	0.38	0.38	0.37	0.35	0.36
C_α atoms	0.43	0.45	0.38	0.39	0.37

[a] Fluctuations are in nanometers.

TABLE 2: Frequencies of Intramolecular Hydrogen Bonds[a] Obtained from Different Simulation Techniques in CPA

donor		acceptor		MD	SD	GLD	SDBEM	GLDBEM
1MeBmt	O−H	10Meleu	O	0	2	3	2	1
2Abu	N−H	5Val	O	16	32	36	26	27
	N−H	11MeVal	O	4	4	4	7	4
5Val	N−H	2Abu	O	67	76	67	64	52
	N−H	3Sar	O	2	1	4	2	2
7Ala	N−H	5Val	O	0	1	2	3	3
	N−H	11MeVal	O	13	51	52	50	45
8Ala	N−H	6MeLeu	O	8	44	43	37	36

[a] Frequencies are in percentages.

Hydrogen-Bonding Analysis. Table 2 reports the results of a hydrogen-bonding (H-bonding) analysis of CPA obtained from MD, SD, GLD, SDBEM, and GLDBEM trajectory data for the last 400 ps. The criteria used to determine a H-bond are purely geometric: for each coordinate set, every potential donor−acceptor pair is tested and considered to form a H-bond if the hydrogen-to-acceptor distance is less than 0.25 nm and the

donor−acceptor angle is larger than 140°. The frequencies of H-bonds are determined from the occurrences registered on the simulation trajectory frames.

In Table 2, eight H-bond donor−acceptor pairs and their occupancies are listed for different simulation approaches. The H-bond occupancies among the pairs 1MeBmt−10MeLeu, 2Abu−11MeVal, 5Val−3Sar, and 7Ala−5Val obtained from the GLDBEM simulation are close or equal to the results from MD simulation. The H-bonds between the pairs 7Ala−11MeVal and 8Ala−6MeLeu in the four stochastic simulations have much higher occupancies than those in the MD simulation. It is found that the residues of 7Ala, 11MeVal, and 8Ala are located at the edge of the loop region. Because the structure of the loop region of CPA in aqueous solution is more open than that of the β-pleated sheet, the internal H-bonds between the pairs 7Ala−11MeVal and 8Ala−6MeLeu in the MD simulation have lower occupancies because of the competition of water molecules for hydrogen-bond donors and acceptors in the solute.

As shown in Table 2, for the H-bonding patterns among the pairs 1MeBmt−10MeLeu, 2Abu−5Val, 5Val−2Abu, 5Val−3Sar, 7Ala−11MeVal, and 8Ala−6MeLeu, the results obtained from the GLDBEM simulation show lower occupancies compared with the data from GLD simulation. In Table 2, it is also found that the H-bond occupancies of the SDBEM simulation are lower compared with those of the SD simulation for the H-bonds between the pairs 2Abu−5Val, 5Val−2Abu, 7Ala−11MeVal, and 8Ala−6MeLeu. This means that the GLDBEM and SDBEM simulations can partially reflect the mean force of the solvent, which imposes an influence on the conformation of the H-bond.

In addition, there are four pairs of H-bonds (1MeBmt−10MeLeu, 2Abu−11MeVal, 7Ala−11MeVal, and 8Ala−6MeLeu) in Table 2 in which the occupancies of the H-bonds obtained from the GLDBEM simulation are closer to those from the MD simulation than to those from the SDBEM simulation. This indicates that the friction memory effect in the GLDBEM simulation also has an influence on the H-bonding network.

Dynamical Behavior. The friction and stochastic terms in the GLE and the hydration force both influence the dynamical properties that can be reflected by the time correlation functions. The time evolution of the atomic positional autocorrelation function has been examined using the following autocorrelation function:

$$c(t) = \frac{\langle \Delta r(t)\, \Delta r(t+\tau)\rangle_\tau}{\langle \Delta r^2\rangle} = \frac{\langle \Delta r(0)\, \Delta r(t)\rangle}{\langle \Delta r^2\rangle} \qquad (29)$$

where the brackets $\langle \cdots \rangle$ represent an average over the simulation time, $\Delta r(t) = r(t) - \langle r\rangle$, and $\langle r^2\rangle = \langle (r - \langle r\rangle)^2\rangle$.

In this study, we have selected two backbone atoms and two side-chain atoms of CPA for analyzing the positional autocorrelation functions for different simulation approaches. Figure 3a−d shows the autocorrelation functions for those four atoms of CPA, in which the backbone atom 7Ala-C_α and the side-chain atom 4Meleu-$C_{\delta 1}$ are in the β-pleated sheet and the backbone atom 10Meleu-C_α and the side-chain atom 10Meleu-$C_{\delta 1}$ are in the loop region. As shown in Figure 3a and b, the correlation functions for backbone atoms 7Ala-C_α and 10Meleu-C_α have a rapid initial decay followed by a linear decrease for all simulations. However, the correlation functions of the GLD and SD simulations in Figure 3b decay even more quickly than those of the other simulations. The correlation function obtained from the GLDBEM simulation in Figure 3b is closer to that obtained from the MD simulation compared with other simula-

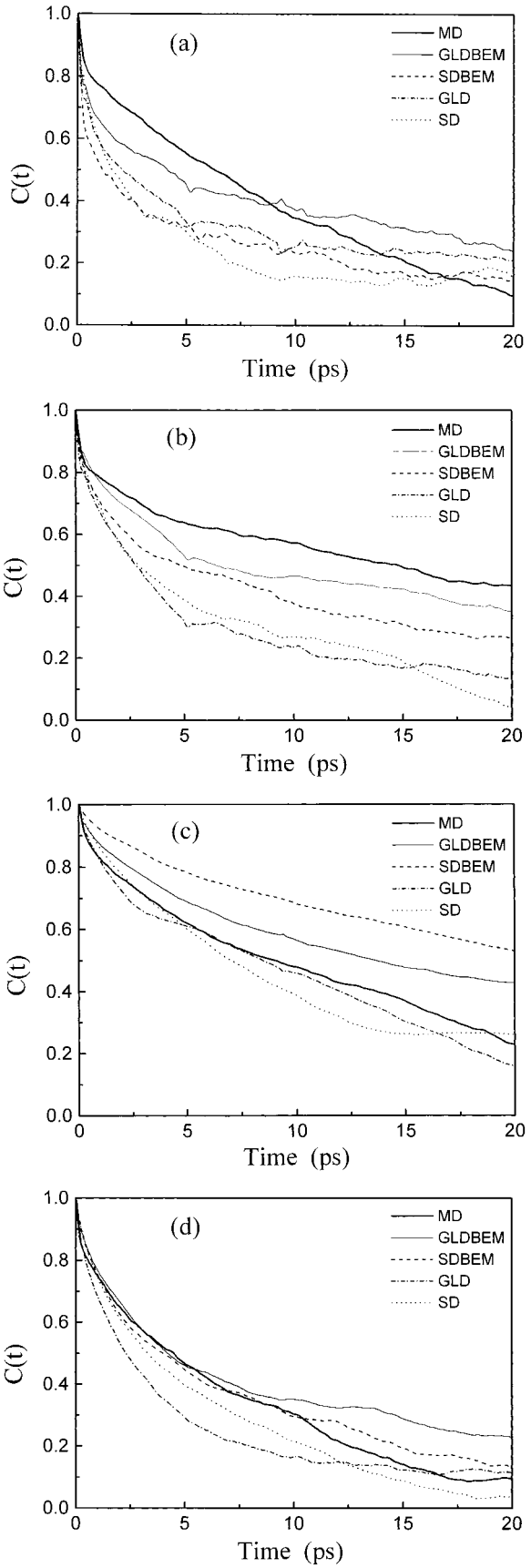

Figure 3. Atomic positional fluctuation autocorrelation functions for four atoms of CPA: (a) 7Ala-C_α, (b) 10MeLeu-C_α, (c) 4MeLeu-$C_{\delta 1}$, and (d) 10MeLeu-$C_{\delta 1}$. The bold solid lines show the MD simulation, the thin solid lines show the GLDBEM simulation, the dashed lines show the SDBEM simulation, the dash-dotted lines show the GLD simulation, and the dotted lines show the SD simulation.

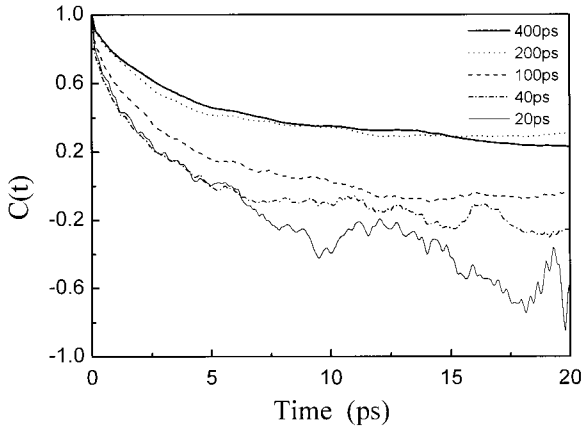

Figure 4. Atomic positional fluctuation autocorrelation functions for 10MeLeu-$C_{\delta 1}$ of CPA for the GLDBEM simulation obtained by averaging for five different simulation times (20, 40, 100, 200, and 400 ps).

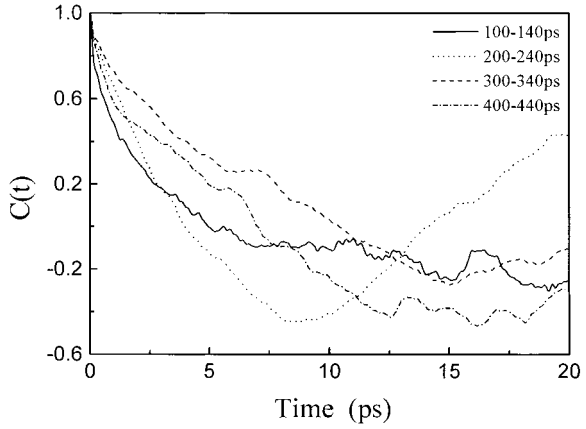

Figure 5. Atomic positional fluctuation autocorrelation functions for 10MeLeu-$C_{\delta 1}$ of CPA for the GLDBEM simulation. The results are obtained by averaging on four different simulation periods in the 500-ps simulation data: solid line, 100−140 ps; dotted line, 200−240 ps; dashed line, 300−340 ps; and dash-dotted line, 400−440 ps.

tions, and the same case can be found in Figure 3a for atom 7Ala-C_α in the early period of 10 ps. This indicates that our GLDBEM simulation for these two backbone atoms gives meaningful results for the correlation functions compared with those of other stochastic simulations. For the atom 10MeLeu-$C_{\delta 1}$ (Figure 3d), the correlation functions obtained from the GLDBEM and SDBEM simulations are very consistent with those obtained from the MD simulation in the early 10-ps period. As shown in Figure 3c for the atom 4MeLeu-$C_{\delta 1}$, the correlation functions of the SDBEM and GLDBEM simulations show even slower decay than those for the MD and other simulations. From the structure analysis mentioned above, the large RMS positional fluctuations of the atom 4MeLeu-$C_{\delta 1}$ can be found in the GLDBEM (0.178 nm) and SDBEM (0.214 nm) simulations. This could be the main reason for the slow decay of the correlation functions shown in Figure 3c for the SDBEM and GLDBEM simulations.

It is interesting to find that the correlation functions of the GLDBEM simulations in Figure 3a−c are closer to those of the MD simulations than to those of the SDBEM simulation. This reflects the influence of the friction memory effect on the atomic dynamical properties of the system. In addition, the correlation functions in Figure 3a−d for the GLDBEM and SDBEM simulations show generally longer relaxation times than those for the SD and GLD simulations. This indicates that the mean force of hydration in the GLDBEM and SDBEM simulations also impose somewhat of an effect on the relaxation time.

It is worth noting that, in our present work, the correlation functions were obtained by averaging on a scale of a 400-ps simulation time, whereas in the previous work,[4,6,7,12] the averaged simulation period was only 40 ps. To understand the difference in the correlation functions obtained from the different simulation time scales, we have analyzed the atomic positional correlation function for the GLDBEM simulation using different simulation times. The results are shown in Figure 4. It is found that the different simulation time scales show very different patterns for the correlation function, the most obvious being an uplifting of all of the correlation function curves, or rather, a slower decay compared with the previous work.[4,6,7,12] This point can be approximately interpreted through the relation between the positional fluctuation and the relaxation time τ of a given atomic fluctuation correlation function, for which the initial decay was approximated by an exponential function. Assuming that the atomic motions of a molecule obey a simple harmonic Langevin equation, the relaxation time τ satisfies the realtion[26,27]

$$\tau = \gamma \frac{\langle \Delta r^2 \rangle}{3 k_B T} \tag{30}$$

where T denotes the temperature, k_B is Boltzmann's constant, $\langle \Delta r^2 \rangle$ represents the positional fluctuation, and γ is the friction coefficient. From our simulation, it is found that the longer the simulation time, the larger the positional fluctuation. Therefore, the results of Figure 4 are consistent with eq 30, in which the 400-ps simulation gave the largest positional fluctuation. Another aspect concerns the stability and reliability of the results. The results for the correlation functions obtained from longer simulations in the present work are more stable than those of the previous work mentioned above.

Here, it is necessary to provide a point of clarification that the closeness between the two curves for the 200-ps and 400-ps simulations in Figure 4 does not imply that there is an upper limit beyond which longer simulations will provide essentially the same positional fluctuation. According to our observations, the curves for different atoms show significantly different patterns; the curve for the 200-ps simulation is not always so close to the curve for the 400-ps simulation. However, they do have a common tendency: the longer the simulation time, the more stable the correlation function curves.

Moreover, when averaged over the same simulation length (40 ps) but at different time sections of the GLDBEM simulation, the correlation functions also show large differences (see Figure 5). This means that the results for analyzing the correlation function using the data from short simulations are less reliable.

Conclusions

In this work, an efficient procedure for combining the BEM with the GLD simulation technique has been described. The two extra mean forces of the hydration force on a charge and the surface pressure of the solvent determined by the BEM and the memory effect of the friction kernel are together taken into account in this method. The analysis results of our GLDBEM simulation have been compared with those of MD, GLD, SD, and SDBEM simulations. The results show that the extra mean force and the friction memory effect of the solvent in the simulations can increase the molecular flexibility and reduce

the total number of intramolecular H-bonds. It was also found that our GLDBEM simulation shows an obvious improvement in dynamical properties compared with conventional SD and SDBEM simulations. In addition, the results for the correlation function obtained from 400-ps simulations in the present work are much more stable than those from the previous 40−60-ps simulations.

We would like to mention that some aspects of the present method could be improved in future work: (1) The calculation speed and precision of the algorithm for solving the Poisson−Boltzmann equations using the BEM and of the numerical integration scheme should be increased. In our work, the simulation CPU time for each picosecond for the CPA molecule on PII233 are as follows: 0.003 h for SD, 0.005 h for GLD, 0.085 h for GLDBEM, and 0.077 h for MD (with 754 water molecules). The computation of solvation forces with the BEM method takes significantly more time than the computation of solute−solvent forces when solvent molecules are explicitly represented. A new algorithm should be explored to accelerate the BEM method. (2) Many MD simulations have shown that the solvent dynamical behavior is bimodal rather than exponential. Therefore, the general form of the GLD simulation should be studied under different models for the friction kernel. (3) The relaxation times of the friction kernels are dependent on atomic species. Therefore, different relaxation times could be selected for the different atoms. (4) The anisotropy of the stochastic force on an atom could be considered because of the anisotropical exposure to solvent molecules.

Acknowledgment. We thank Professor W. F. van Gunsteren for kindly providing the GROMOS package. C.X.W. thanks the Abdus Salam International Centre for Theoretical Physics (ICTP), Trieste, Italy, because this work was done (in part) in the framework of Associate Membership Program of the ICTP. This work was supported in part by the Chinese Natural Science Foundation (No. 19774501, No. 29992590-2) and the Beijing Natural Science Foundation (No. 5992002).

References and Notes

(1) Karplus, M.; Petsko, G. A. *Nature* **1990**, 347, 631.
(2) van Gunsteren, W. F.; Weiner, P. K.; Wilkinson, A. J. *Computer Simulation of Biomolecular Systems: Theoretical and Experimental Application*; Leidon ESCOM: The Netherlands, 1993; Vol. 2.
(3) Smith, J. C.; Karplus, M. *J. Am. Chem. Soc*. **1992**, 114, 801.
(4) Wang, C. X.; Wan, S. Z.; Xiang, Z. X.; Shi, Y. Y. *J. Phys. Chem*. **1997**, 101, 230.
(5) Fraternali, F.; van Gunsteren, W. F. *J. Mol. Biol*. **1996**, 256, 939.
(6) Lautz, J.; Kessler, H.; van Gunsteren, W. F.; Weber, H. P.; Wenger, R. M. *Biopolymers* **1990**, 29, 1669.
(7) Shi, Y. Y.; Wang, L.; van Gunsteren, W. F. *Mol. Simul*. **1988**, 1, 369.
(8) Zauhar, R. J. *J. Comput. Chem*. **1991**, 12, 575.
(9) Sharp, K. *J. Comput. Chem*. **1991**, 12, 454.
(10) Gilson, M. K.; Davis, M. E.; Luty, B. A.; McCammon, J. A. *J. Phys. Chem*. **1993**, 97, 3591.
(11) Gilson, M. K.; McCammon, J. A.; Madura, J. D. *J. Comput. Chem*. **1995**, 16, 1081.
(12) Wan, S. Z.; Wang, C. X.; Shi, Y. Y. *Mol. Phys*. **1998**, 93, 901.
(13) Xiang, Z. X.; Huang, F. H.; Shi, Y. Y. *J. Phys. Chem*. **1994**, 98, 12782.
(14) Kubo, R. *Rep. Prog. Phys*. **1966**, 29, 255.
(15) Vesely, F. J. *Mol. Phys*. **1984**, 53, 505.
(16) van Gunsteren, W. F.; Berendsen, H. J. C. *Mol. Simul*. **1988**, 1, 173.
(17) Papoulis, A. *Probability, Random Variables and Stochastic Processes*; 2nd ed.; McGraw-Hill: New York, 1985.
(18) Yoon, B. J.; Lenhoff, A. M. *J. Comput. Chem*. **1990**, 11, 1080.
(19) Zauhar, R. J.; Morgan, R. S. *J. Mol. Biol*. **1985**, 186, 815.
(20) Juffer, A. H.; Botta, E. F. F.; van Keulen, B. A. M.; Ploeg, A. V. D.; Berendsen, H. J. C. *J. Comput. Phys*. **1991**, 97, 144.
(21) van Gunsteren, W. F.; Berendsen, H. J. C. Groningen Molecular Simulation (GROMOS) Library Manual, BIOMOS: Groningen, The Netherlands, 1987.
(22) Loosli, H. R.; Kessler, H.; Oschkinat, H.; Weber, H. P.; Petchez, T. J.; Widmer, A. *Helv. Chim. Acta* **1985**, 68, 661.
(23) Daggett, V.; Levitt, M. *Annu. Rev. Biophys. Biomol. Struct*. **1993**, 22, 353.
(24) Berendsen, H. J. C.; Postma, J. P. M.; van Gunsteren, W. F.; DiNola, A.; Haak, J. R. *J. Chem. Phys*. **1984**, 81, 3684.
(25) Ryckaert, J. P.; Ciccotti, G.; Berendsen, H. J. C. *J. Comput. Phys*. **1977**, 23, 327.
(26) Chandrasekchar, S. *Rev. Mod. Phys*. **1943**, 15, 1.
(27) Swaminathan, S.; Ichiye, T.; van Gunsteren, W. F.; Karplus, M. *Biochemistry* **1982**, *21*, 5230.